

# Monte Carlo Convolution for Learning on Non-Uniformly Sampled Point Clouds

PEDRO HERMOSILLA, Ulm University, Germany

TOBIAS RITSCHEL, University College London, United Kingdom

PERE-PAU VÁZQUEZ and ÀLVAR VINACUA, Universitat Politècnica de Catalunya, Spain

TIMO ROPINSKI, Ulm University, Germany

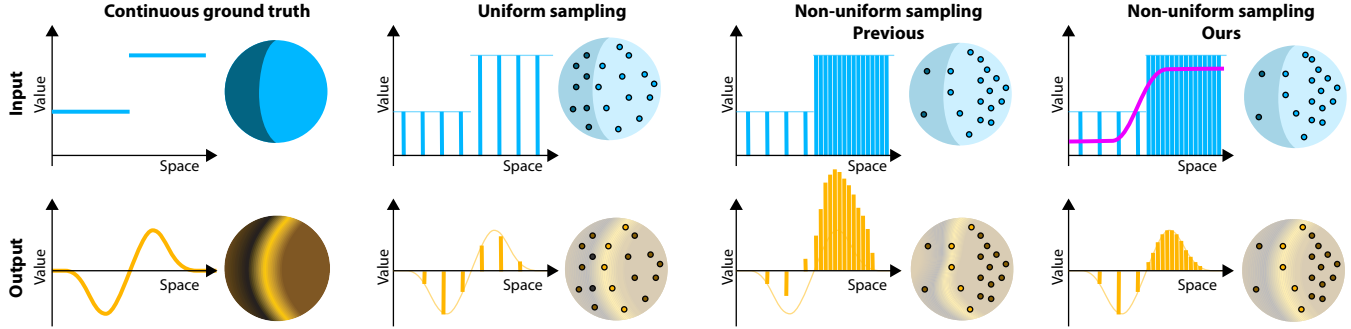


Fig. 1. Non-uniform sampling, which is inherent to most real-world point cloud datasets, has a severe impact on the convolved result signal. An input signal represented as 1D function and as projected on a 3D sphere (**top row**) is convolved with an edge-detection kernel to obtain the resulting signal represented as 1D function and as projected on a 3D sphere (**bottom row**). The four columns illustrate the impact of the sample distribution on the convolution result. The ground truth continuous signal’s filter response (**first column**) is faithfully captured when convolving uniformly sampled point clouds (**second column**). In the case of non-uniformly sampled point clouds, state-of-the-art convolutional methods severely deviate from the desired filter response (**third column**). With our interpretation of non-uniform convolution as a Monte Carlo estimate in respect to a given sample density distribution (illustrated by the pink line), we can compensate this deviation and obtain a filter response faithfully capturing that of the ground truth (**fourth column**).

We propose an efficient and effective method to learn convolutions for non-uniformly sampled point clouds, as they are obtained with modern acquisition techniques. Learning is enabled by four key novelties: first, representing the convolution kernel itself as a multilayer perceptron; second, phrasing convolution as a Monte Carlo integration problem, third, constructing an unstructured Poisson disk hierarchy for pooling, and fourth, using Monte Carlo convolution as pooling and upsampling operation at different resolutions simultaneously. The key idea across all these contributions is to guarantee adequate consideration of the underlying non-uniform sample distribution function from a Monte Carlo perspective. To make the proposed concepts applicable for real-world tasks, we furthermore propose an efficient implementation which significantly reduces the required GPU memory. By employing our method in hierarchical network architectures we can outperform most of the state-of-the-art networks on established point cloud segmentation, classification and normal estimation benchmarks. Furthermore, in contrast to most existing approaches, we can also demonstrate the robustness of our method with respect to sampling variations even when only trained on uniformly sampled models.

Additional Key Words and Phrases: Deep learning; Convolutional neural networks; Point clouds; Monte Carlo integration

Authors’ addresses: Pedro Hermosilla, Ulm University, Germany, pedro-1.hermosilla-casajus@uni-ulm.de; Tobias Ritschel, University College London, United Kingdom, t.ritschel@ucl.ac.uk; Pere-Pau Vázquez, Àlvar Vinacua, Universitat Politècnica de Catalunya, Spain; Timo Ropinski, Ulm University, Germany, timo.ropinski@uni-ulm.de.

## 1 INTRODUCTION

We describe a new approach for learning on non-uniformly sampled point clouds. While convolutional neural networks have achieved unprecedented performance when learning on structured data [He et al. 2015; Huang et al. 2016; Wang et al. 2017], their application to unstructured data such as point clouds is still fairly new. Early methods have looked into fully-connected approaches and striven for permutation and rotational invariance [Guerrero et al. 2018; Qi et al. 2017a,b]. Follow up work has proposed several extensions [Atzmon et al. 2018; Graham and van der Maaten 2017; Groh et al. 2018; Huang et al. 2018; Li et al. 2018; Shen et al. 2017; Su et al. 2018; Wang et al. 2017, 2018; Xu et al. 2018; Yu et al. 2018]. Unfortunately, the non-uniform sampling typically associated with real-world point cloud data, such as for instance resulting from the projective effect of a LiDAR scan, has not been a special focus of previous research. As this uniform sampling results in severe implications, as illustrated in Fig. 1, the proposed approach has been developed with a special focus on non-uniformly sampled point clouds. Nevertheless, it still achieves competitive performance on uniformly sampled data.

To make progress towards our goals, we take into account the original definition of convolution as an integral, and its meaning when evaluated in an unstructured setting. By phrasing convolution as a Monte Carlo estimate of this integral, we will show that proper handling of the underlying sampling density is crucial, and when done properly, can produce results surpassing the state-of-the-art,

yet with a simple and natural definition and an easy implementation. To this end we make four key contributions.

First, representing the convolution kernel itself as a multilayer perceptron (MLP). Since a convolution kernel maps a spatial offset (Laplacian) to a scalar weight, representing and learning this mapping through an MLP is a natural choice. This notion is inherently invariant under translation (as it works on relative values), and normalizing the Laplacian by the receptive field size leads to scale-invariance.

Second, we suggest using Monte Carlo integration to compute unstructured convolutions. Key is the adequate handling of non-uniform and varying-density points from a Monte Carlo (MC) point of view. Weighted summing pairs of points formally means to sample an MC estimate of an integrand. While MC requires to divide by the probability of each sample, in the uniform setting this results in a division by a constant which thus can be omitted. However, when dealing with a varying sample density as present in non-uniformly sampled point clouds, failing to perform this normalization leads to bias and consequently reduced learning ability. Therefore, we claim our approach to provide a new form of *sampling invariance*, where for instance simply duplicating a point will not change the estimated integrand. Stating convolution as MC integration allows us to tap into the rich machinery of MC, including (quasi) randomization [Niederreiter 1992] and importance sampling [Kahn and W. Marshall 1953]. Furthermore, the convolution is invariant under point re-orderings and typically works on receptive fields with a variable number of neighboring points.

Third, our approach employs a multi-resolution pooling strategy based on Poisson disk sampling [Wei 2008]. This allows us to extract features at multiple spatial scales while preserving the non-uniform sampling. Starting from the original point cloud, we define point clouds with fewer points, where the local point density is a fraction of the original point density, while the mutual distances retain a Poisson disk property. Currently-used farthest point sampling would quickly produce a uniform-density sampling.

Fourth, we introduce MC pooling and up-sampling operations. We compute the point features at level  $l$  by performing a convolution using its points as centers and points from level  $l + i$  as source function. These operations enable us to determine the features of level  $l$  based on features of several levels at the same time.

We demonstrate the outcome of our approach, which is based on these four novelties, by comparing it against state-of-the-art point cloud learning techniques when performing point cloud segmentation, classification, and normal estimation. We will show that we outperform the state-of-the-art when learning on non-uniform point clouds, while we still achieve state-of-the-art performance for uniformly sampled point clouds.

**Overview.** After introducing previous work in Sec. 2, we present the four key components to enable learning on non-uniformly sampled signals: Representing the convolution kernel as a MLP (Sec. 3), evaluating the convolution integral by using MC (Sec. 4), using a Poisson Disk hierarchy (Sec. 5), and pooling by using convolutions on different levels (Sec. 6). Then, in Sec. 7 we discuss how these components are able to process non-uniformly sampled point clouds, and in Sec. 8 we present a GPU implementation, which allows the application of these concepts to real-world point clouds. Lastly, in

Sec. 9, we evaluate the proposed method wrt. the state-of-the-art by performing point cloud segmentation, classification, and normal estimation.

## 2 PREVIOUS WORK

A straight-forward method to enable learning on point clouds, is to resample them to a regular grid, before applying learning approaches developed for structured data. While extensions to multiple resolutions exist e. g., based on octrees [Wang et al. 2017], we will solely focus on those techniques directly learning on unstructured data. On the following paragraphs we will describe the most relevant works in the field.

PointNet [Qi et al. 2017a] pioneered deep learning on such unstructured datasets. It used a fully-connected network together with a clever machinery to achieve rotation and permutation-invariance. PointNet++ [Qi et al. 2017b] added extension to localized sub-networks, but was not yet fully convolutional. PCP Net [Guerrero et al. 2018] allowed for inference of local properties like curvature or normals, but was also not convolutional.

Klokov and Lempitsky [2017] presented a convolutional learner, which uses a  $k$ -d tree. However, since the leaf nodes of the tree have a fixed number of points, it is sensitive to varying density, being tight to the logic of building and querying  $k$ -d tree. In contrast, our approach in uses only linear-time hashing to access neighbors and thus works on multiple scales.

Shen et al. [2017] also provide a translation-invariant but non-convolutional method, where convolution is replaced with correlation of local neighborhood graphs with learned graph templates. While showing good performance on small problems, it likely does not scale well and remains particularly sensitive to the underlying graph structure.

Dynamic Graph CNNs by Wang [2018] are convolutional. They employ a fairly general notion of learnable operations on edges of a graph of neighboring points. Different from other approaches, they change neighborhoods during learning. This makes the approach slightly more complex to implement and likely not efficient on large point clouds.

PointCNN [Li et al. 2018] is also convolutional, working on the  $k$  nearest neighbors. They represent the entire convolution as an MLP (so for  $k$  neighbors such an MLP has  $k$  inputs), while we represent only the kernel function as an MLP, with much fewer parameters, independent of  $k$ .

SPLATNet [Su et al. 2018] seeks inspiration from the permutohedral lattice [Adams et al. 2010], where convolutions can efficiently be performed on sparse data in high dimensions, while the filter kernels are discrete masks in lattice space. Uneven sample distributions in the lattice are addressed by convolving the 1 [Adams et al. 2010]. Our work achieves the same, but without the complication of creating a lattice.

Atzmon et al. [2018] use radial basis functions defined on discrete set of points to represent the convolution kernel. The work is mathematically involved but provides invariance under global re-sampling by construction and evaluates it. However, sampling non-uniformity is not considered.

In concurrent work, SpiderCNN [Xu et al. 2018] uses step functions to represent convolutions. They mention using the MLPs we

use as well, but found them to perform worse than step functions. In combination with our other contributions, we found MLPs to perform well. We acknowledge further work shall explore different continuous representations to parametrize learned convolutions.

Other pre-print work by Groh et al. [2018] suggests to use a linear function as a representation of an unstructured convolution kernel. With considerations how dis-similar 2D convolution kernels are from linear functions, we think an MLP to describe a kernel is worth exploring. Thanks to the simplicity we share in our approach, they demonstrate excellent scalability to millions of points, such as ours, but the problem of non-uniform sampling is not touched upon.

Most of the existing methods are based on convolving the  $k$  nearest neighbors (using a hierarchical structure or not) [Groh et al. 2018; Klovov and Lempitsky 2017; Li et al. 2018; Shen et al. 2017; Wang et al. 2018; Xu et al. 2018]. This approach is not robust to non-uniform samplings, since adding more points into a region in the space will reduce the  $k$  nearest neighbors to a small volume around each point, capturing different features from those the kernel was trained on. Aztmom et al. [2018], although not considering non-uniformity in their paper, transform the point cloud to volumetric functions which can be robust to non-uniformly sampled point clouds. However, several computations of their method are quadratic on the number of points which makes their method not scalable. PointNet++ [Qi et al. 2017b], although using a sampling algorithm quadratic in the number of point, computes features locally, making it scalable. Moreover, it was tested with non-uniformly sampled point clouds by simulating a LIDAR scan. However, their method selects a fixed number of random samples within a radius around the points and it does not consider the point density in its computations, which, as we will demonstrate, can lead to errors.

### 3 CONVOLUTION KERNELS

Within this section we will first recall the definition of a convolution (Sec. 3.1) before we introduce how to represent convolution kernels by using MLPs (Sec. 3.2). By using our MLP representation, efficient and simple to train, non-linear filtering of irregular data becomes possible.

#### 3.1 Convolution as an integral

Recall the definition of a convolution as an integral of a product:

$$(f * g)(\mathbf{x}) = \int f(\tau)g(\mathbf{x} - \tau)d\tau \quad (1)$$

where  $f$  is a scalar function on  $\mathbb{R}^3$  we want to convolve and  $g$  is the *convolution kernel*, a scalar function on  $\mathbb{R}^3$ . In our particular case,  $f$ , is the *feature function*, for which we have a set of discrete samples  $\mathbf{x}_i$  (our data points). If for each point no other information is provided besides its spatial coordinates,  $f$  represents the binary function which evaluates to 1 at the sampled surface and 0 otherwise. However,  $f$  can represent any type of input information such as color, normals, etc. For internal convolutions, which are subsequent to the input layer, it can also be features from a previous convolution.

*Translation-invariance.* As the value of  $g$  only depends on relative positions, convolution is translation-invariant.

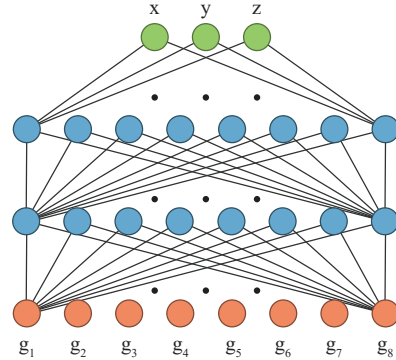


Fig. 2. Representation of convolution kernels  $g_i$  by a multilayer perceptron (MLP) of two hidden layers of 8 neurons each. In order to reduce the number of parameters and computations, each MLP outputs values of 8 different convolution kernels ( $g_1, \dots, g_8$ ).

*Scale-invariance.* Since evaluating the integral in Equation 1 on the entire domain can be prohibitive for large datasets, we limit the domain of  $g$  to a sphere centered at 0 and radius 1. In order to support multiple radii, we normalize the input of  $g$  by dividing it by the convolution’s radius  $r$ . In particular, we choose  $r$  to be a fraction of the scene bounding box diameter  $b$ , for instance  $r = .01 \cdot b$ . Doing so results in scale-invariance.

*Rotation-invariance.* Note, that we do not achieve and seek to achieve any rotation-invariance. Typical image convolutions are not rotation invariant either and succeed nonetheless.

#### 3.2 Multilayer perceptron kernels

We suggest to represent the kernel  $g$ , by a multilayer perceptron (MLP).

*Definition.* This MLP takes as input the spatial offset  $\delta = (\mathbf{x} - \tau)/r$  comprising of three coordinates, normalized by dividing by the radius of the convolution  $r$ . The output of the MLP is a single scalar. To tradeoff accuracy and performance, we use two hidden layers of 8 neurons each (see Section Sec. 9 for more details). In the following, we denote the hidden parameters as a vector  $\omega$ .

For layers with a high number of input and output features, the number of kernels, and therefore the number of parameters the network has to learn, is too high ( $\#inputs \times \#outputs$ ). In order to address this problem, we use the same MLP to output 8 different  $g$ ’s, thus reducing the number of MLP’s by a factor of 8. Figure 2 presents an illustration of one of our MLP’s.

*Back-propagation.* For back-propagation [Rumelhart et al. 1986], the derivative of a convolution with respect to the parameter  $\omega_l$  of the MLP is

$$\frac{\delta f * g}{\delta \omega_l} = \int f(\tau) \frac{\delta g(\mathbf{x} - \tau)}{\delta \omega_l} d\tau. \quad (2)$$

#### 3.3 Single and multi-feature convolution

Our convolution consumes  $M$  input feature functions and outputs  $L$  convolved feature functions. Based on the way the convolved feature functions are calculated, we define two types of layers: *Single-feature*

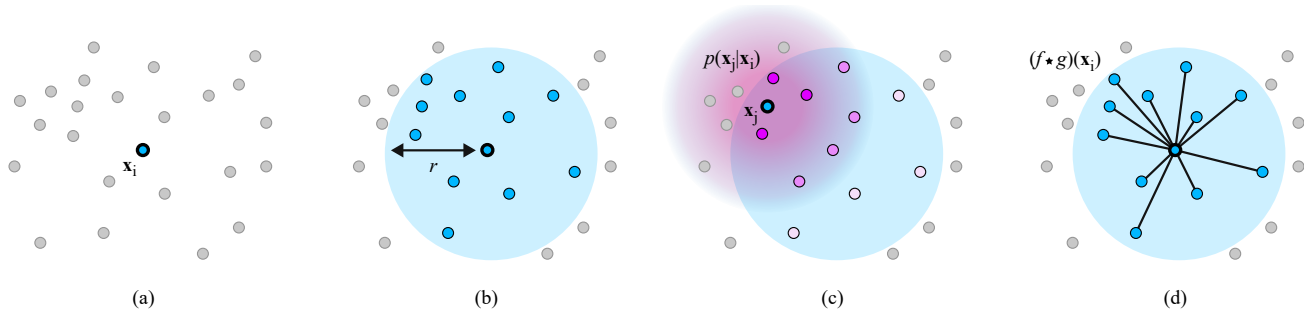


Fig. 3. Steps of our spatial convolution. For a given point  $\mathbf{x}_i$  (**Figure a**) the neighbors within radius  $r$  are retrieved from our acceleration data structures (**Figure b**). For each neighboring point  $\mathbf{x}_j$ , its probability density function,  $p(\mathbf{x}_j|\mathbf{x}_i)$ , is computed using *Kernel Density Estimation* [Parzen 1962; Rosenblatt 1956]. **Figure c** illustrates this process, in which the *bandwidth* is represented by a pink circle and the intensity of the colors on the neighboring points represents their effect on the computation of  $p(\mathbf{x}_j|\mathbf{x}_i)$ . Lastly, the convolution at point  $\mathbf{x}_i$  is evaluated using Monte Carlo integration (**Figure d**).

spatial convolution (ssconv) and *Multi-feature* spatial convolution (msconv). Single-feature spatial convolution outputs a scalar feature by convolving a scalar input feature. Therefore, in these layers, the number of output features is equal to the number of input features,  $M = L$ , and the number of kernels  $g$  is also equal to  $M$ . The multi-feature convolution, on the contrary, is similar to the layers used in standard convolutional neural networks where, each output feature is computed as the sum of all input feature functions convolved:

$$f_o = \sum_{i=0}^M f_i * g_{o,i} \quad (3)$$

These layers are more computationally demanding since they have to learn  $M \times L$  convolution kernels  $g$ .

## 4 MONTE CARLO CONVOLUTION

In this section, we will show how convolutions can be stated as a Monte-Carlo estimate by relying on a sample’s density function, which ultimately makes learning robust to non-uniform sample distributions.

### 4.1 Monte Carlo integration

In order to compute the convolution in each sample point, we have to evaluate the integral of Equation 1. Since we only have a set of samples of our function  $f$ , we propose to compute this integral by using MC integration [Kalos and Whitlock 1986], which uses a set of random samples to compute the value of an integral.

*Definition.* In our case, these samples comprise of the input data points or a (quasi) random subset. Therefore, an estimate of the convolution for a point  $\mathbf{x}_i$  is

$$(f * g)(\mathbf{x}_i) \approx \frac{1}{|\mathcal{N}(\mathbf{x}_i)|} \sum_{j \in \mathcal{N}(\mathbf{x}_i)} \frac{f(\mathbf{x}_j)g\left(\frac{\mathbf{x}_i - \mathbf{x}_j}{r}\right)}{p(\mathbf{x}_i|\mathbf{x}_j)}, \quad (4)$$

where  $\mathcal{N}(\mathbf{x}_i)$  is the set of neighborhood indices in a sphere of radius  $r$ , and  $p(\mathbf{x}_j|\mathbf{x}_i)$  is the value of the *Probability Density Function* (PDF) at point  $\mathbf{x}_j$  when the point  $\mathbf{x}_i$  is fixed, i. e., the convolution is computed at  $\mathbf{x}_i$ . Figure 3 provides an illustration of this computation.

Please note, that since our input data points are non-uniformly distributed, each point  $\mathbf{x}_j$  will have a different value of  $p(\mathbf{x}_j|\mathbf{x}_i)$ . In simple words, if a point was duplicated,  $p$  would increase. Correctly accounting for this effect is key to our approach.

It is also worth noticing, that the PDF depends not only on the sample position  $\mathbf{x}_j$  but also on  $\mathbf{x}_i$ : How likely it is to draw a point does not only depend on the point itself, it also depends on how likely the others in the receptive field of radius  $r$  are.

Please finally note, that here, and in the following,  $\mathbf{x}_i$  is an arbitrary point, that might not be from the set of all  $\mathbf{x}_j$ . This property will later allow re-sampling to other levels or other irregular or regular domains.

*Back-propagation.* Back-propagation [Rumelhart et al. 1986] in respect to the MLP parameters  $\omega_l$  can also be estimated using MC:

$$\left(\frac{\delta f * g}{\delta \omega_l}\right)(\mathbf{x}_i) = \frac{1}{|\mathcal{N}(\mathbf{x}_i)|} \sum_{j \in \mathcal{N}(\mathbf{x}_i)} \frac{f(\mathbf{x}_j)}{p(\mathbf{x}_j|\mathbf{x}_i)} \frac{\delta g\left(\frac{\mathbf{x}_i - \mathbf{x}_j}{r}\right)}{\delta \omega_l}. \quad (5)$$

### 4.2 Estimating the PDF

Regrettably, the sample density itself is not given, but must be estimated from the samples themselves. Fortunately, this can be done using Kernel Density Estimation [Parzen 1962; Rosenblatt 1956]. This function is high where the samples are dense and low when they are sparse. It is estimated as

$$p(\mathbf{x}_j|\mathbf{x}_i) \approx \frac{1}{|\mathcal{N}(\mathbf{x}_i)|\sigma^3} \sum_{k \in \mathcal{N}(\mathbf{x}_i)} \left\{ \prod_{d=1}^3 h\left(\frac{\mathbf{x}_{jd} - \mathbf{x}_{kd}}{\sigma}\right) \right\}, \quad (6)$$

where  $\sigma$  is the bandwidth which determines the smoothing of the resulting sample density function (we use  $\sigma = .25r$ ),  $h$  is the Density Estimation Kernel a non-negative function whose integral equals 1 (we use a Gaussian), and  $d$  is one of the three dimensions of  $\mathbb{R}^3$ .

The PDF of a point  $\mathbf{x}_j$  in respect to a given point  $\mathbf{x}_i$  is always relative to all other samples in the receptive field. Therefore, density can not be pre-computed for a point  $\mathbf{x}_j$  since its value will be different for each receptive field defined by  $\mathbf{x}_i$  and radius  $r$ . Note, that in a uniform setting,  $p$  is a constant.

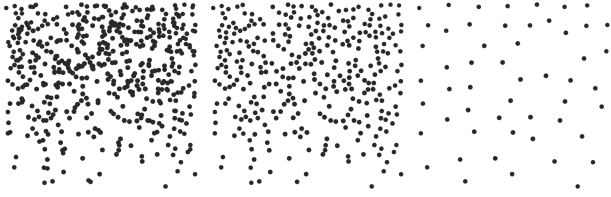


Fig. 4. Point clouds resulting of iteratively applying our Poisson disk sampling algorithm on a model of a plane with variable point density along the  $y$  axis (**left**). Note how in the first layer (**middle**) the point densities are preserved whilst the at the last level (**right**) the model is represented by only a few points uniformly distributed over the initial model.

## 5 POISSON DISK HIERARCHY

Deep neural networks that want to benefit from both local and global information routinely reduce – and later increase again – the image resolution by using pooling operations. This is done on point clouds in our approach, such that the non-uniform sampling density is preserved on the first resolutions and the coarse point sets retain a uniformly distributed coverage of the space.

Our spatial pooling layers, which are designed analogous to conventional structured pooling layers, receive as input  $N$  points and output  $N'$  points, being  $N' < N$ . Although, random sampling could be used to reduce the number of samples in a point cloud, when applying it to non-uniformly sampled point clouds chances are high, that some features will not be faithfully represented at coarse levels. While other methods, such as farthest point sampling, would be able to handle this problem, they do not scale well. Thus, in our spatial pooling layer, we instead ensure a Poisson disk distribution [Cook 1986] of samples and allow a variable density of points over the space. These layers execute the Parallel Poisson Disk Sampling algorithm [Wei 2008] and output a sample distribution with a Poisson disk equal to  $r_p$ , where  $r_p$  is an input parameter of the layer. The output of our sampling algorithm generates a point cloud in which the minimum distance between points is  $r_p$ , by removing points at smaller distances and preserving points at distances higher than  $r_p$ . By iteratively applying these operations on a point cloud, we generate a model with fewer points during each iteration. We iterate this process until we obtain a point cloud composed of only a few points uniformly distributed over the original model. Figure 4 shows the different point clouds obtained after applying our sampling strategy to a point cloud representing a sphere with variable point density.

Note that, contrary to other sampling approaches, this technique generates a non-fixed number of samples. Therefore, our networks cannot take advantage of acceleration techniques commonly used by deep learning frameworks in which the memory required for a forward pass is reserved in advance. However, we still achieve good performance as is presented in Section 9.4.

## 6 MONTE CARLO POOLING

After having established a coarse point cloud, we need to pool the features from the fine point cloud. Convolutional neural networks designed to process images commonly use two types of operations in their pooling layers, max pooling and average pooling. Max pooling selects the maximum value for each feature among the values

of the pixels within a window in image space. By using a similar approach, in our continuous space with overlapping spheres, could lead to biases when the same value is shared among two neighboring spheres. Average pooling, on the contrary, can be efficiently implemented in our scenario as an integral evaluated using MC. However, in our implementation, we decided to define the pooling operation as a convolution, allowing to learn a different pooling operation for each feature.

Our pooling layers transfer features from a point cloud  $l$  with  $N$  points to another point cloud  $l + i$  with  $N'$  points, being  $N > N'$ . Qi et al. [2017b] computed the new features on points from model  $l + 1$  by selecting points within a certain radius from model  $l$  and use their features as input to their PointNet networks. Similar to this approach, our pooling operations use points from model  $l + i$  as the center of our MC convolutions, while convolving the features from points of model  $l$ . By doing so, our pooling operations pass features from one level to another by transforming them using learnable convolutions.

Qi et al. [2017b] limited the use of these layers to pooling operations of two consecutive levels in the point hierarchy. However, this definition of pooling operations not only allows us to compute features of sub-sampled point clouds, but also allows us to perform upsampling operations. The operation is identical to the pooling layer. However, in this case, the source point cloud  $l$  is composed of fewer samples than point cloud  $l + i$ , instead of having more points. These pooling and upsampling convolutions can be understood as learnable encoder and decoder kernels.

As these operations have no restriction on the point clouds  $l$  and  $l + i$  used, we will be able to compute point features from multiple levels of the hierarchy at the same time.

## 7 NON-UNIFORMITY HANDLING

When processing non-uniformly sampled point clouds, enough points must lie in the receptive field of a convolution layer, such that MC integration is meaningful. When enough points are present, using the PDF to weight the contribution of each point results in the same feature value independently of the point distribution used to compute it. However, when the point density in an area is too small, and thus too few points are within the receptive field of our convolutions, incorrect results might occur since the number of samples provided are not enough to correctly approximate the convolution integral. This problem could be solved by increasing the convolution radius. However, by doing so we can obtain poor performance since, depending on the sampling density, the number of points within the receptive field can be high in another areas of the model.

In order to solve this problem, we convolve features at different resolutions of our Poisson disk hierarchy. Thus, when computing features on a point, we use a similar approach as Qi et al. [2017b], i.e., we compute features at different resolution by using different radii on our convolutions. However, Qi et al. [2017b] used the same point set to compute all the operations. They selected a fixed number of random points within the receptive field in order to prevent processing too many and obtain poor computational speed. This can lead to incorrect results when the distribution of points is not uniform over the receptive field, in which case most of the points can be selected from the area with higher density. To address this

problem, we use a different approach. We use different levels of our Poisson Disk sampling to compute the convolutions at different resolutions. For local features, we use the first levels of the hierarchy and a small radius. However, to capture features at bigger scales, we use a bigger convolution radius and a deep level of our hierarchy which is composed of a small number of points following a Poisson disk distribution. This idea can be used to upsample features from different resolutions in Encoder-Decoder network architectures, or to compute the class probabilities from point clouds with different resolutions in classification networks (see Section Sec. 9).

## 8 IMPLEMENTATION

In this section, we describe several implementation details of the building blocks of our networks.

*PDF computation.* Our implementation differs from averaging the individual contributions of the neighboring points only by the requirement to divide by their probability values  $p$ . Therefore, our MC approach requires two steps: computing all values of  $p$  and querying them when MC-convolving.

To compute  $p$ , we create a hashed voxel grid as proposed by Teschner et al. [2003] with cell size  $r$  in time and space linear in the number of points.

For lookup performance, the neighbor indices  $\mathcal{N}(x_i)$  of a point  $i$  are stored in  $N$  flat lists. Additionally, we compute the values of  $p(x_j|x_i)$  and store them in a list of the same size. Both lists can get arbitrarily long with arbitrarily high density, which decreases performance during the computation of our convolution for large values of  $r$ . However, maintaining a good ratio between the radius of the convolution and the Poisson disk radius of the point set, provides an upper bound number of possible neighbors for each point.

Based on the previous data structures, the neighbor indices, as well as the PDF, can now be looked-up in constant time using the computed information. When looking up the neighbor values, they are multiplied by the kernel weight  $g(x_j - x_i)/r$  and divided by the  $p(x_j|x_i)$ .

Note that the voxel grid in which points are distributed, is computed in parallel on the GPU, resulting in different point orderings within the same cell for different executions. This introduces randomness in the output sampled point clouds of our Poisson disk sampling strategy, which is preferred during learning. Section Sec. 9 evaluates the effect of the randomness on the resulting accuracy.

*Multilayer Perceptron Evaluation.* Evaluating the MLP during MC convolutions requires a considerable amount of GPU memory when using the implementation provided by standard frameworks. This limits the number of computed features per point and the number of convolutions used in the network architecture. In order to address these limitations, we implemented the MLP evaluation in a single GPU kernel. By doing so, our networks do not require to expand the features and coordinates of neighboring points and they do not require either to store intermediate MLP results for each layer. However, with this implementation, we are not able to use some features, such as batch normalization, to improve learning.

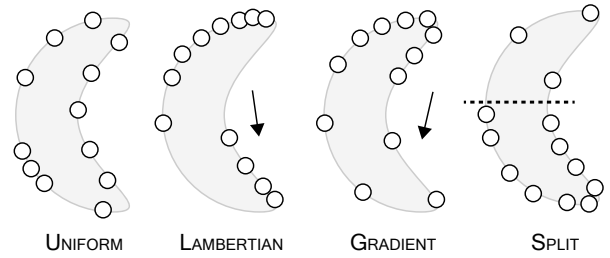


Fig. 5. UNIFORM is uniformly random. LAMBERTIAN depends on the orientation, here shown as an arrow and locations facing this direction are more likely to contain points. For GRADIENT, the likelihood of generating a point decreases along a direction, here shown as an arrow again. For SPLIT, the shape is split into two halves, here shown as a dotted line, where each part is samples uniformly random, but with different density.

*Batch Processing.* Our layers process point clouds of variable size. Moreover, as described in Section 4, our convolutions take into account all the neighboring points to carry out their computations. These design choices do not allow us to use the standard tensor approach to process a batch of models in parallel.

In order to support batch processing, we use an extra vector with an integer value for each point that describes the model identifier to which the point belongs. We create a regular grid for each model and during the evaluation of the layers, only the appropriate data structure is updated and queried based on this identifier. This simple approach allows us to process batches of models with variable size in parallel by increasing the memory consumption linearly with the number of points. However, in configurations with reduced GPU memory, a more sophisticated approach can be considered, such as only storing the number of points per model and perform extra computations in the layers.

## 9 EVALUATION

Here we report the results obtained when using the machinery explained before in a complete network on specific data for relevant tasks. To make the reported results comparable, we introduce a dataset with non-uniform sampling in Sec. 9.1 based on current benchmark data. Next, we describe the notation (Sec. 9.2), before reporting actual quantitative evaluation results we obtained for specific tasks in Sec. 9.3.

### 9.1 Non-uniformly sampled test data

Non-uniform test data is found in typical scanned scenes. However, existing benchmarks provide data sets of uniformly sampled models [Wu et al. 2015; Yi et al. 2016]. In order to evaluate the performance of our and other state-of-the-art networks we generated our own data set by artificially producing non-uniform samplings (see Fig. 5).

To produce such data, we start from a uniformly sampled point cloud, and at each point perform rejection sampling, whereby the rejection probability is computed according to one of four protocols: UNIFORM (no rejection), SPLIT (probability is either a random constant smaller than 1 in a random half-space or 1, we used 0.25 in our tests), GRADIENT (probability is proportional to the projection

Table 1. Comparison of the performance achieved by the state-of-the-art methods for the classification, segmentation, and normal estimation tasks. The performance for the classification task is measured in percentage of correct predictions, for the segmentation task by the intersection over union metric, and for the normal estimation by mean cosine loss (distance). Our network architectures are able to **outperform** most of the state-of-the-art techniques in the segmentation and normal estimation task, and achieve state-of-the-art results in the classification task.

	Classify	Segment	Normals
<sup>1,2</sup> [Su et al. 2018]	-	85.1	-
<sup>1</sup> [Xu et al. 2018]	<b>92.4 %</b>	85.3	-
<sup>1</sup> [Qi et al. 2017b]	91.9 %	85.1	.47
[Qi et al. 2017a]	89.2 %	83.7	-
[Groh et al. 2018]	90.2 %	-	-
[Shen et al. 2017]	90.8 %	84.3	-
[Wang et al. 2018]	92.2 %	85.1	-
[Li et al. 2018]	91.7 %	<b>86.1</b>	-
[Atzmon et al. 2018]	92.3 %	85.1	.19
[Klokov and Lempitsky 2017]	91.8 %	82.3	-
MC (Ours)	91.4 %	85.9	<b>.16</b>

<sup>1</sup> Additional input

<sup>2</sup> One network per class in segmentation tasks

onto the largest bounding box axis), and LAMBERTIAN (probability is proportional to the clamped dot product between the surface normal and a fixed “view” direction). These sampling protocols are applied during the testing phase on the data sets of the different benchmarks. Thus, each time a model is loaded, we apply one of these sampling techniques (depending on which one we are currently testing) with a random seed to generate the probabilities of each point and the view direction in the Lambertian case.

## 9.2 Notation

In order to describe architectures making use of our novel layers, we will use the following notation:

- `msconv` (#1, #2, #3, #4): Multi-feature convolution with #1 output features per point and radius #2, using level #3 of the hierarchy as center of the convolution and level #4 as the samples of the feature functions to convolve.
- `ssconv` (#1, #2, #3, #4): Single-feature convolution with #1 output point features and radius #2, using level #3 of the hierarchy as center of the convolution and level #4 as the samples of the feature functions to convolve.
- `full` (#1, #2): Fully connected layer which combines #1 input features to generate #2 output features.

## 9.3 Tasks

In this section, we describe the methods and network architectures used to carry out all three tasks, classification, segmentation, and normal estimation.

**9.3.1 Classification.** Our network architectures used for classification, are composed of several levels, whereby each computes a convolution on a point cloud, uses Poisson disk sampling to reduce

the number of points, and performs a downsampling operation to compute the features of the sub-sampled points. Figure 6 illustrates these architectures.

The spatial convolution of the first level is a multi-feature convolution in order to increase the number of features per point. However, in deeper levels, we use a single-feature convolution for performance considerations. These types of convolutions compute a point feature based on only one input feature, which can reduce the learning ability of our networks. In order to incorporate combinations of features in such levels, we introduce a fully connected layer between the spatial convolutions, which generates new features per point by combining the input features. This layer can be understood as a  $1 \times 1$  convolution in the context of convolutional neural networks for images.

Before each layer, we add a batch normalization layer to improve training, and a ReLU layer to introduce non-linearities into the input. Moreover, similar to Dense blocks in DenseNets [Huang et al. 2016], we incorporate skip links between the output of the downsampling layers and the output of the spatial convolution.

The final output of the network is a global feature vector describing the model which is processed by an MLP with two hidden layers.

**Methods.** In order to evaluate the performance of our classification network architecture we used the re-sampled version of the ModelNet 40 dataset [Wu et al. 2015] provide by Qi et al. [Qi et al. 2017a]. This dataset is composed of 12,311 point clouds uniformly sampled from man-made objects of 40 different categories. The official train/test split is composed of 9,843 models in the train set and 2,468 in the test set. We trained our network, MCClass in Figure 6, on this dataset using 1,024 points per model. During testing, the models were sampled into 1,024 points according to the protocol of Section 9.1

MCClass generates a point cloud hierarchy of four levels by iteratively using Poisson Disk sampling on the input point cloud with radius .1, .4, and  $\sqrt{3}$  (we use as the first level the original point cloud). The network is composed of three different levels as is illustrated in Figure 6, and each of them perform the following operations:

- 1: `msconv` (64, .1, 1, 1)  $\rightarrow$  `full` (64, 128)  $\rightarrow$  `ssconv` (128, .2, 2, 1)
- 2: `ssconv` (128, .4, 2, 2)  $\rightarrow$  `skiplink`  $\rightarrow$  `full` (256, 512)  $\rightarrow$  `ssconv` (512, .8, 3, 2)
- 3: `ssconv` (512, 1.1, 3, 3)  $\rightarrow$  `skiplink`  $\rightarrow$  `full` (1024, 2048)  $\rightarrow$  `ssconv` (2048,  $\sqrt{3}$ , 4, 3)

The last level of the hierarchy (4) is composed of only a single point since the Poisson Disk radius used to compute it was equal to the diagonal of the bounding box. The global feature vector is then processed by an MLP with two hidden layers of 1024 and 512 neurons, and 40 outputs, where 40 is the number of existing categories. This network was trained and tested with 1024 points per model for comparison purposes.

Moreover, we also trained another network architecture, MCClassH in Figure 6. This network was designed to increase the robustness of the classification under poor sampling density models, sacrificing some accuracy on uniformly sampled point clouds. As the previous network, MCClassH computes a point cloud hierarchy of four levels

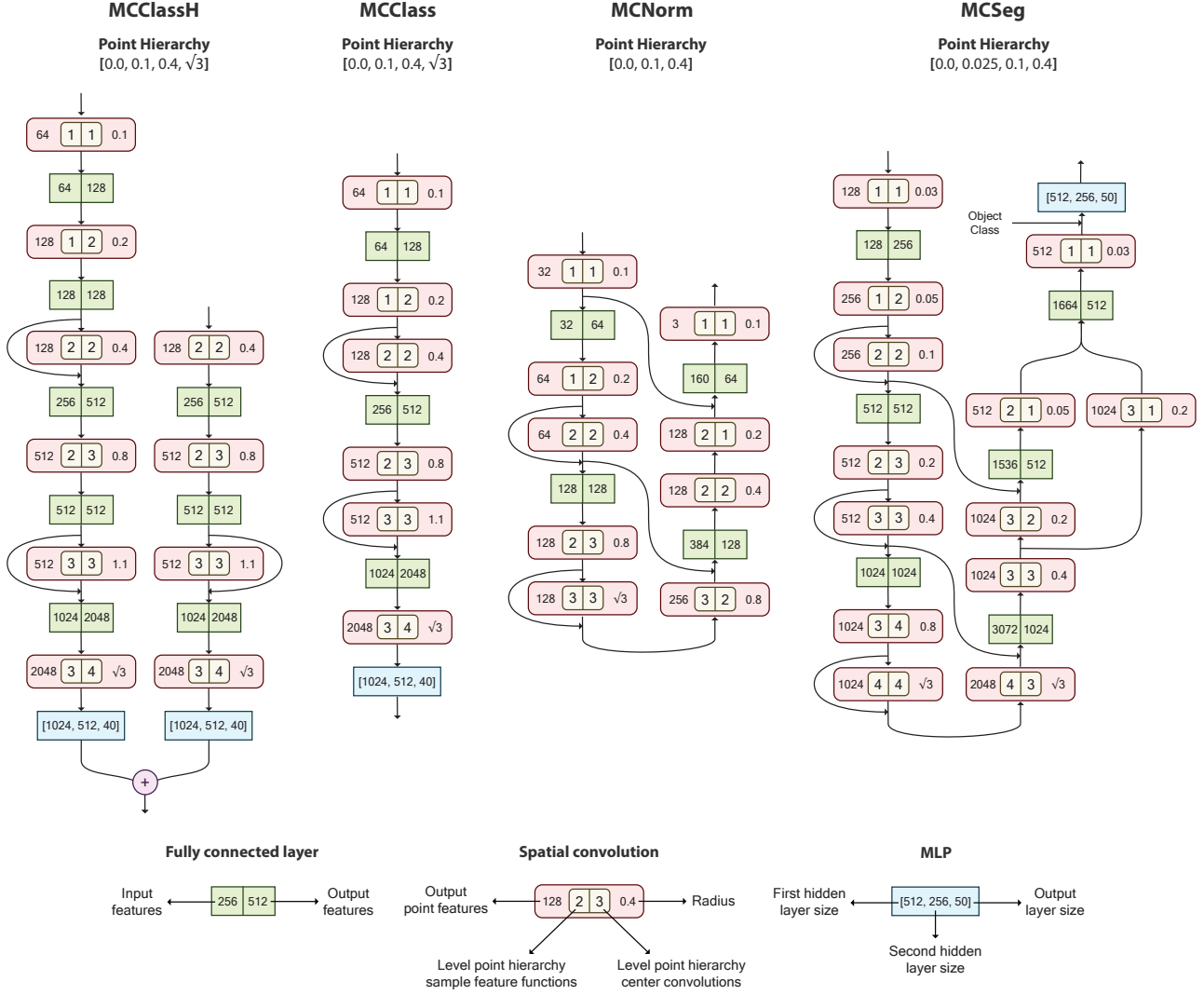


Fig. 6. Network architectures used for the classification (MCClassH and MCClass), normal estimation (MCNorm), and segmentation tasks (MCSeg). For each network the point hierarchy used is also provided as a list of Poisson Disk radii used in each level. Note that the radius of the first level is always 0.0 since this level is composed of the initial point set. The three different building blocks used to generate our networks are described at the bottom of the figure: Spatial convolutions, which use a level of the point hierarchy as the center of the convolution and another level to sample the feature functions in order to generate a set of new point features; Fully connected layers, which reduce or increase the number of point features by combining them; And multi layer perceptron (MLP), which is composed of 3 fully connected layers. Note that in all networks the first convolutions are multi-layer convolutions since they increase the number of features. Moreover, in the MCNorm network, the last convolution is a multi-layer convolution since it reduces the number of features to the 3 dimensions of the output normals. The rest of convolutions are single-feature convolutions.

using the same Poisson disk radius. Then, two different paths generate different probability vectors which are added together to create the final class probabilities (see Figure 6). The first path is similar to the MCClass network:

- 1: msconv (64, .1, 1, 1)  $\rightarrow$  full (64, 128)  $\rightarrow$  ssconv (128, .2, 2, 1)
- 2: full (128, 128)  $\rightarrow$  ssconv (128, .4, 2, 2)  $\rightarrow$  skiplink  $\rightarrow$  full (256, 512)  $\rightarrow$  ssconv (512, .8, 3, 2)
- 3: full (512, 512)  $\rightarrow$  ssconv (512, 1.2, 3, 3)  $\rightarrow$  skiplink  $\rightarrow$  full (1024, 2048)  $\rightarrow$  ssconv (2048,  $\sqrt{3}$ , 4, 3)

The second path is composed of only two layers and works directly with the second level of the point cloud hierarchy:

- 1: msconv (128, .4, 2, 2)  $\rightarrow$  skiplink  $\rightarrow$  full (256, 512)  $\rightarrow$  ssconv (512, .8, 3, 2)
- 2: full (512, 512)  $\rightarrow$  ssconv (512, 1.2, 3, 3)  $\rightarrow$  skiplink  $\rightarrow$  full (1024, 2048)  $\rightarrow$  ssconv (2048,  $\sqrt{3}$ , 4, 3)

During training, we deactivate one or none of the two paths. Moreover, in order to evaluate our MC convolutions, we trained a version of our MCClass network, AVG, in which the convolutions



Table 2. Comparison of the accuracy of our networks, MClass and MClassH, with the accuracy of PointNet++ [Qi et al. 2017b] (PN++) on the ModelNet40 classification tasks using different sampling strategies. Whilst PN++ obtained a slightly better performance than network MClass on the SPLIT dataset, MClass performed better on the GRADIENT sampling strategy where the points inside the receptive field along the whole model do not follow a uniform distribution. However, our network MClassH, outperformed PN++ in both cases. On the LAMBERT dataset, all networks achieved a similar performance. Measurements for an MClass network trained averaging the individual contributions of the points within the receptive field instead of using Monte Carlo (AVG) are also reported, demonstrating the improvement introduced by our operations.

	Classification			
	MClassH	MClass	AVG	PN++
UNIFORM	90.9 %	<b>91.4 %</b>	89.4 %	89.1 %
SPLIT	<b>87.6 %</b>	82.3 %	81.4 %	84.4 %
GRADIENT	<b>87.3 %</b>	83.5 %	81.9 %	79.7 %
LAMBERT	73.0 %	74.3 %	71.6 %	<b>74.6 %</b>

are computed without dividing by the PDF of each point. This can be understood as simply averaging the individual contributions of the point within the receptive field.

Lastly, we trained the same network, MClass, with MLP of different sizes in order to evaluate its effect in the final accuracy. We trained three networks, the first one with MLPs composed of 4 neurons per layer with 4 outputs, the second one with MLPs composed of layers with 8 neurons and 8 outputs, and the last one with MLPs of 16 neurons per layer and 16 outputs.

To counterbalance the randomness introduced by the Parallel Poisson Disk Sampling algorithm, each measure was taken by averaging the results of 5 independent executions of our networks.

*Training.* In order to train our classification networks, we used cross-entropy loss with an Adam optimizer, a batch size equal to 32, and an initial learning rate of .005. Every 20 epochs we divided the learning rate by half. To prevent over-fitting we used a drop-out probability of .5 in the final MLPs, a drop-out probability of .2 for the point features before each layer, and a weight decay equal to .00001 for the MClass network. Moreover, we selected a point from the dataset with a probability of .95, which varied the 1,024 input points during training. We trained our network for 200 epochs on an Nvidia GTX 1080 Ti.

*Analysis.* As it is illustrated in Table 1, our approach generates competitive results, achieving 91.4 % of accuracy with the network MClass. Table 2 also illustrates that network MClassH obtained a similar performance, 90.9 %. Moreover, our networks presented a robust performance on non-uniformly sampled point clouds (see Table 2). MClass outperformed PointNet++ [Qi et al. 2017b] on the GRADIENT protocol by 3.8 % (MC 83.5 % vs. PN++ 79.7 %), which demonstrated the robustness of our approach on variable point densities. PointNet++, on the contrary, due to the random point selection during their sphere sampling, it is not able to capture variable point density. However, our method presented smaller performance in the SPLIT protocol than PointNet++ (MC 82.3 % vs. PN++ 84.4 %). The better performance of PointNet++ on this sampling protocol

Table 3. Comparison of the accuracy obtained in the classification task for different sizes of our MLPs (4, 8, and 16 neurons per layer). The maximum accuracy was obtained by the MLP with layers of 8 neurons, whilst the MLP with layers of 4 achieved the smaller timing. We decided to use 8 neurons for the layers of our MLPs since it is a good trade-off between accuracy and execution time.

	MLP size evaluation		
	MLP4	MLP8	MLP16
Accuracy (%)	89.9 %	91.4 %	90.5 %
Timing (ms)	16.3	17.8	20.1

can be explained by the bigger radius used at the first level, better capturing the features of the poorly (but uniformly) sampled areas well.

MClassH, however, presented the better performance on both SPLIT and GRADIENT datasets (87.6 % and 87.3 %). By deactivating one or none paths during training, the network is able to classify objects based on the original point cloud with high resolution, and it is also able to compensate the error introduced by poorly sampled areas by using the second path.

For the LAMBERT protocol, all networks presented a similar performance of around 74 – 73 %. In this protocol, half the points for each model are missing which makes the correct classification of the object difficult.

Furthermore, when compared with the AVG network, our MC convolutions obtained better performance on all protocols as is presented in Table 2. Moreover, the AVG network had more difficulties to generalize, as compared with our MClass network, presenting sever overfitting.

The variance of the resulting accuracy over several executions of the network MClass was .0367, proving that, despite the random point selection of our sampling layers, the resulting accuracy is stable.

Lastly, when comparing the results obtained with different MLP sizes, we found out that 8 neurons per layer achieved the best accuracy maintaining a small execution time (see Table 3).

*9.3.2 Segmentation.* As one of the evaluations, we investigated the results obtained on point cloud segmentation. The network architecture used for this task is composed of an encoder and a decoder part. As illustrated in Figure 6, the encoder is a classification network. The decoder network, on the contrary, can be seen as a mirrored classification network. Levels on the decoder are composed by an upsampling layer, a fully connected layer, and a spatial convolution.

In order to prevent vanishing gradients and thus improve learning, we incorporate skip links [Ronneberger et al. 2015] between the encoder and the decoder levels. Moreover, in the last level of the decoder, we compute the upsampled features from two different levels at the same time, providing features at different scales for each point.

The output of the network is a feature vector per point which is then processed by an MLP of two hidden layers.

*Methods.* We used an instance of our segmentation network architecture to segment the point clouds of the ShapeNet dataset [Yi

et al. 2016]. This dataset contains 16,881 point clouds uniformly sampled from 16 different classes of objects, each one composed of between 2 and 6 parts, making a total of 50 parts. We use the standard train/test split for training [Qi et al. 2017b], and the class of the point cloud is assumed for this task. We used as input of our networks the complete point clouds, which are in the range of 1,000 to 3,000 points per object. As in the classification task, in order to evaluate the performance of our networks with non-uniformly sampled datasets, we selected 2,048 points from each model during testing based on the probabilities described in Section 9.1.

We trained one network, MCSEg in Figure 6, for this task. This network first computes a four-level hierarchy point cloud by iteratively applying our Poisson disk sampling algorithm with radius .025, .1, and .4. The layers of such network perform the following operations on the computed point hierarchy:

- E1: msconv (128, .03, 1, 1)  $\rightarrow$  full (128, 256)  $\rightarrow$  ssconv (256, .05, 2, 1)
- E2: ssconv (256, .1, 2, 2)  $\rightarrow$  skiplink  $\rightarrow$  full (512, 512)  $\rightarrow$  ssconv (512, .2, 3, 2)
- E3: ssconv (512, .4, 3, 3)  $\rightarrow$  skiplink  $\rightarrow$  full (1024, 1024)  $\rightarrow$  down (1024, .8, 4, 3)
- E4: ssconv (1024,  $\sqrt{3}$ , 4, 4)  $\rightarrow$  skiplink
- D3: ssconv (2048,  $\sqrt{3}$ , 3, 4)  $\rightarrow$  skiplink  $\rightarrow$  full (3072, 1024)  $\rightarrow$  ssconv (1024, .4, 3, 3)
- D2: ssconv (1024, .2, 2, 3)  $\rightarrow$  skiplink  $\rightarrow$  full (1536, 512)  $\rightarrow$  ssconv (512, .1, 2, 2)
- D1: (ssconv (1024, .2, 3, 1) | ssconv (512, .05, 2, 1))  $\rightarrow$  skiplink  $\rightarrow$  full (1664, 512)  $\rightarrow$  ssconv (512, .03, 1, 1)

Since the class of the model is assumed as input, as in PointNet++ [Qi et al. 2017b], we concatenate a *one-hot* vector containing this information with the output of our network. This information is processed by an MLP composed of two hidden layers with 512 and 256 neurons, and 50 outputs, where 50 is the number of parts.

Moreover, as in the classification task, we evaluate the effect of the MC convolutions by training a version of our MCSEg network using AVG convolutions.

*Training.* We trained this network using cross-entropy as loss function with an Adam optimizer and a batch size of 32. We used an initial learning rate of .005 which was scaled by .2 every 20 epochs. As in the classification networks, we used a drop out rate of .5 in the final MLP and .2 before each layer. Since in this task we used the complete point set as input, we used a probability of .2 to drop out a point during training. We trained our network for 90 epochs on an Nvidia Quadro P6000.

*Analysis.* Table 1 presents the performance achieved by our segmentation network. The performance was measured using the mean Intersection Over Union metric as in Yi et al. [2017]. Our network presented competitive results when compared with state-of-the-art methods, only slightly surpassed by PointCNN [Li et al. 2018]. Our method achieved 85.9 whilst PointCNN achieved 86.1. Note that PointCNN is based on  $k$  nearest neighbors convolutions, and, as discussed in Section Sec. 2, is not the best approach to handle non-uniformly sampled point clouds. Moreover, we compared the performance of our network to the performance of PointNet++ [Qi et al. 2017b] (see Table 4). Our network obtained better results on the

Table 4. Comparison of the performance obtained with our segmentation network, MCSEg, and the performance obtained with PointNet++ measured using the Intersection Over Union metric. Whilst our network is able to obtain better performance than the state of the PointNet++ on uniformly sampled point clouds, on the SPLIT and GRADIENT dataset both networks achieved similar results. On the LAMBERT dataset, however, our network obtain better performance. We also compared our network with the same architecture using average convolutions (AVG). Although MCSEg obtained a better result on uniformly sampled data, both networks obtained similar performance on the non-uniformly sampled datasets.

	Segmentation		PN++
	MCCSeg	AVG	
UNIFORM	<b>85.9</b>	85.6	84.9
SPLIT	84.6	<b>84.9</b>	84.8
GRADIENT	<b>84.0</b>	83.8	83.8
LAMBERT	82.7	<b>83.1</b>	77.5

LAMBERT protocol than PointNet++ (MC 82.7 vs PN++ 77.5). On the other protocols, however, both networks obtained a similar performance. MCSEg performed slightly better on our GRADIENT protocol (MC 84.0 vs PN++ 83.8) whilst on the SPLIT protocol PointNet++ performed slightly better (MC 84.6 vs PN++ 84.8).

When comparing with the AVG network, MCSEg presented higher accuracy on the uniformly sampled protocol (MC 85.9 vs AVG 85.6) and on the GRADIENT protocol (MC 84.0 vs AVG 83.8). However, the AVG network performed better on the SPLIT (MC 84.6 vs AVG 84.9) and LAMBERT protocols (MC 82.7 vs AVG 83.1). Nevertheless, the differences between these two networks are small.

*9.3.3 Normal estimation.* We also test our networks in a normal estimation task. Whereas classification and segmentation tasks require to output probabilities and use them to determine the class or part id, normal estimation requires more fine computations in which a small modification of the output values is relevant to the correctness of the result.

Since the output is generated for each vertex we use a similar architecture as for our segmentation networks (see Figure 6). However, for this task we removed the last MLP, generating the actual normals by a final convolution with 3 outputs.

*Methods.* Similar to Atzmon et al. [2018], we used the dataset ModelNet 40 to evaluate our network, taking 1,024 points from each model and using the standard train/test split.

We use a network with an encoder-decoder architecture, MCNorm in Figure 6, which generates a point hierarchy of 3 levels by iteratively applying our Poisson Disk Sampling algorithm with radius .1 and .4. This network performs the following operations on this hierarchy:

- E1: msconv (32, .1, 1, 1)  $\rightarrow$  full (32, 64)  $\rightarrow$  ssconv (64, .2, 2, 1)
- E2: ssconv (64, .4, 2, 2)  $\rightarrow$  skiplink  $\rightarrow$  full (128, 128)  $\rightarrow$  ssconv (128, .8, 3, 2)
- E3: ssconv (128,  $\sqrt{3}$ , 3, 3)  $\rightarrow$  skiplink
- D2: ssconv (256, .8, 2, 3)  $\rightarrow$  skiplink  $\rightarrow$  full (384, 128)  $\rightarrow$  ssconv (128, .4, 2, 2)
- D1: ssconv (128, .2, 1, 2)  $\rightarrow$  skiplink  $\rightarrow$  full (160, 64)  $\rightarrow$  msconv (3, .1, 1, 1)

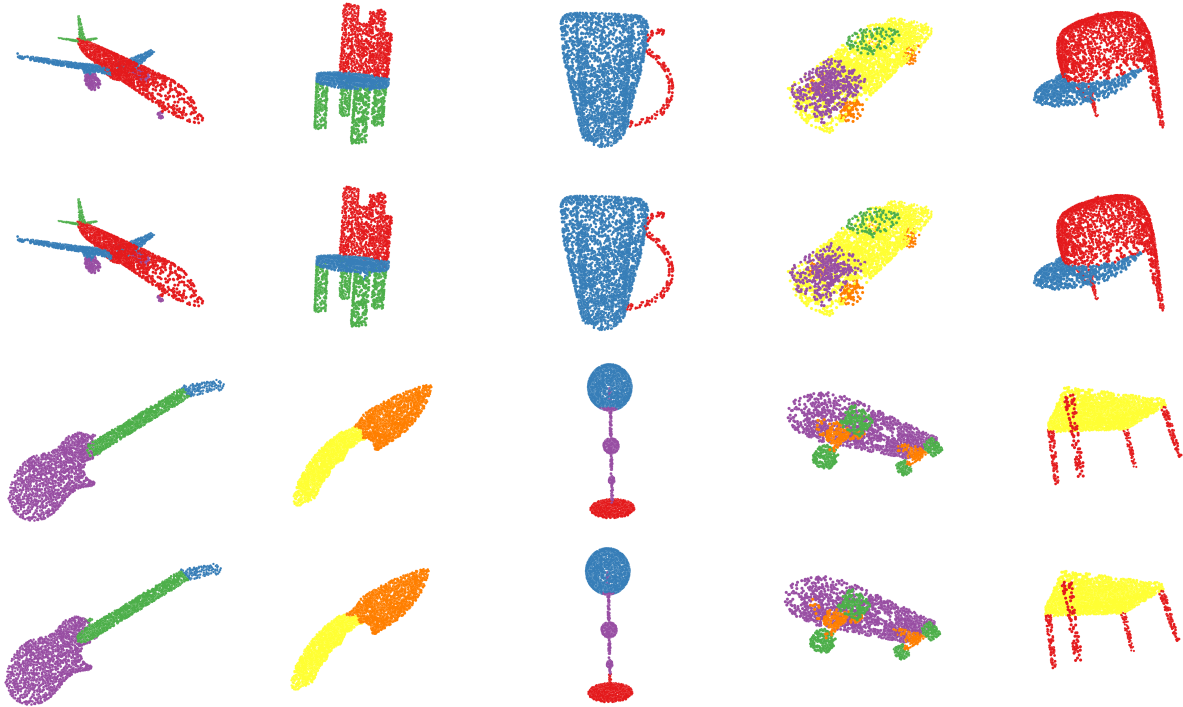


Fig. 7. Comparison of the resulting segmentation generated by using our MCseg network (first and third row) with the ground truth (second and fourth row).

Moreover, we trained a version of this network using average convolution (AVG).

Lastly, in order to evaluate the MC convolutions without considering the Poisson Disk hierarchy we trained two simple networks composed of two convolutions (MCNormS):  $\text{msconv}(32, .1, 1, 1) \rightarrow \text{msconv}(3, .1, 1, 1)$ . One network was trained using MC convolutions and the other one using average convolutions (AVGS).

*Training.* We used the cosine distance loss function to train our network using an Adam optimizer and a batch size of 16. Initially, we used a learning rate of .005 which we decreased by half every 20 epochs. We trained our network MCNorm for 160 epochs and MCNormS for 45 epochs on an Nvidia GTX 1080 Ti.

*Analysis.* Table 1 presents the results obtained by our network compared with state of the art. Our network outperformed the state of the art methods, achieving a mean cosine distance of .16 and improving thus the accuracy reported by Atzmon et al. [2018] (.19).

Moreover, we also compared the performance of our network on the non-uniformly sampled protocols (See Table 5). Our network, MCNorm, outperformed in all protocols to PointNet++ [Qi et al. 2017b], demonstrating thus that considering the probability distribution function of the point set is crucial to achieve good performance in tasks which the outputs of the network are real values instead probabilities.

The same network with average convolutions obtained a good performance. However, as in the other tasks, the networks trained with MC convolutions obtained better results.

Table 5. Comparison of the mean cosine distance obtained during normal estimation task with different network architectures. Our network MCNormS outperformed the state-of-the-art in all the sampling protocols tested. Moreover, this network obtained better results than the same network trained using average convolutions (AVG). Moreover, we trained two small networks composed of only two convolutions with MC convolutions (MCNormS) and average convolutions (AVGS). MCNormS was able to generalize better than AVGS, achieving better results than AVGS on all datasets.

	Normal Estimation				
	MCNorm	AVG	PN++	MCNormS	AVGS
UNIFORM	<b>.161</b>	.165	.469	.282	.305
SPLIT	<b>.204</b>	.220	.581	.312	.336
GRADIENT	<b>.201</b>	.215	.616	.310	.334
LAMBERT	.716	.743	1.61	<b>.662</b>	.693

The results obtained with MC convolutions on network MCNormS were also better than the ones obtained with average convolutions in all protocols. Moreover, this network (trained only for a few epochs) was able to obtain better results than the ones achieved by PointNet++. Also note that network MCNormS achieved small cosine error than MCNorm for the LAMBERT protocol. This is due to the fact that the initial and final convolutions of MCNormS uses a bigger radius than the ones in MCNorm.

#### 9.4 Network timing

Table 6 presents the time required to train an epoch of our networks and the time in milliseconds to compute a forward pass for a single

Table 6. Computation time of our method for different tasks. Training time is measured for one single epoch. Testing time is the time required to process a forward pass of an individual model.

	Training	Testing	GPU
Classification	244 s	17.8 ms	Nvidia GTX 1080i
Segmentation	2359 s	89.4 ms	Nvidia P6000
Normal estimation	426 s	28.1 ms	Nvidia GTX 1080i

model. Due to our parallel implementation of all the algorithms and our acceleration data structures, all networks present competitive performance. The lowest performance was reported by the MCseg network since it requires to compute a high number of features for the initial point set. Measurements for networks MCclass, and MCnorm were obtained using an Nvidia GTX 1080 Ti, whilst the measurements for the MCseg network were obtained with an Nvidia Quadro P6000 since this network requires more GPU memory during training.

## 10 CONCLUSIONS

We have shown how phrasing convolution, for learning on non-uniformly sampled point clouds, as a MC estimate produces results superior to the state-of-the-art in typical learning-based processing of point clouds, such as segmentation, classification and normal estimation, while it at the same time simplifies the representation. This was enabled by representing the convolution kernel itself using a multilayer perceptron, by treating convolution as a MC estimate with a proper sample density function, by using Poisson disk pooling, and by realizing MC up- and down-sampling to preserve the original sample density.

In future work, we would like to study different architectures and the effect of the hyper-parameters. Moreover, we would like to apply our idea to inputs of higher dimensionality, such as animated point clouds, point clouds with further attributes on them such as color. Another direction for future research could be to consider what a non-uniform density means when dealing with triangular or tetrahedral meshes, that also typically do not come with uniform sampling.

## ACKNOWLEDGEMENTS

The authors thank the Ulm University Center for Translational Imaging MoMAN for its support, the Spanish Ministerio de Economía y Competitividad, and 839 FEDER (EU) for partially funding this research under the Grant No. TIN2017-88515-C2-1-R. Furthermore, we would like to acknowledge NVidia’s GPU donation for our training cluster.

## REFERENCES

Andrew Adams, Jongmin Baek, and Myers Abraham Davis. 2010. Fast High-Dimensional Filtering Using the Permutohedral Lattice. In *Computer Graphics Forum*, Vol. 29. 753–762.

Matan Atzmon, Haggai Maron, and Yaron Lipman. 2018. Point Convolutional Neural Networks by Extension Operators. *SIGGRAPH 2018* (2018).

Robert L. Cook. 1986. Stochastic Sampling in Computer Graphics. *ACM Trans. Graph.* 5, 1 (Jan. 1986), 51–72. <https://doi.org/10.1145/7529.8927>

Benjamin Graham and Laurens van der Maaten. 2017. Submanifold Sparse Convolutional Networks. (2017). arXiv:arXiv:1706.01307

Fabian Groh, Patrick Wieschollek, and Hendrik P. A. Lensch. 2018. Flex-Convolution (Deep Learning Beyond Grid-Worlds). (2018). arXiv:arXiv:1803.07289

Pau Guerrero, Yanir Kleiman, Maks Ovsjanikov, and Niloy J. Mitra. 2018. PCPNet: Learning Local Shape Properties from Raw Point Clouds. *Eurographics* (2018).

Kaiming He, Xiangyu Zhang, Shaoqing Ren, and Jian Sun. 2015. Deep Residual Learning for Image Recognition. *CoRR abs/1512.03385* (2015). arXiv:1512.03385

Gao Huang, Zhuang Liu, and Kilian Q. Weinberger. 2016. Densely Connected Convolutional Networks. *CoRR abs/1608.06993* (2016). arXiv:1608.06993

Qiangui Huang, Weiyue Wang, and Ulrich Neumann. 2018. Recurrent Slice Networks for 3D Segmentation of Point Clouds. *Proc. Computer Vision and Pattern Recognition (CVPR), IEEE* (2018).

H Kahn and A W. Marshall. 1953. Methods of Reducing Sample Size in Monte Carlo Computations. 1 (11 1953), 263–278.

Malvin H. Kalos and Paula A. Whitlock. 1986. *Monte Carlo Methods*. Wiley-Interscience, New York, NY, USA.

Roman Klokov and Victor Lempitsky. 2017. Escape from cells: Deep kd-networks for the recognition of 3d point cloud models. In *ICCV*. 863–72.

Yangyan Li, Rui Bu, Mingchao Sun, and Baoquan Chen. 2018. PointCNN. (2018). arXiv:arXiv:1801.07791

Harald Niederreiter. 1992. *Random Number Generation and quasi-Monte Carlo Methods*. Society for Industrial and Applied Mathematics, Philadelphia, PA, USA.

Emanuel Parzen. 1962. On Estimation of a Probability Density Function and Mode. *Ann. Math. Statist.* 33, 3 (09 1962), 1065–1076.

Charles R Qi, Hao Su, Kaichun Mo, and Leonidas J Guibas. 2017a. PointNet: Deep Learning on Point Sets for 3D Classification and Segmentation. *Proc. Computer Vision and Pattern Recognition (CVPR), IEEE* (2017).

Charles R Qi, Li Yi, Hao Su, and Leonidas J Guibas. 2017b. PointNet++: Deep Hierarchical Feature Learning on Point Sets in a Metric Space. *arXiv preprint arXiv:1706.02413* (2017).

Olaf Ronneberger, Philipp Fischer, and Thomas Brox. 2015. U-Net: Convolutional Networks for Biomedical Image Segmentation. In *Medical Image Computing and Computer-Assisted Intervention – MICCAI 2015*, Nassir Navab, Joachim Hornegger, William M. Wells, and Alejandro F. Frangi (Eds.). Springer International Publishing, Cham, 234–241.

Murray Rosenblatt. 1956. Remarks on Some Nonparametric Estimates of a Density Function. *Ann. Math. Statist.* 27, 3 (09 1956), 832–837.

David E Rumelhart, Geoffrey E Hinton, and Ronald J Williams. 1986. Learning representations by back-propagating errors. *Nature* 323, 6088 (1986), 533.

Yiru Shen, Chen Feng, Yaoqing Yang, and Dong Tian. 2017. Mining Point Cloud Local Structures by Kernel Correlation and Graph Pooling. (2017). arXiv:arXiv:1712.06760

Hang Su, Varun Jampani, Deqing Sun, Subhansu Maji, Evangelos Kalogerakis, Ming-Hsuan Yang, and Jan Kautz. 2018. SPLATNet: Sparse Lattice Networks for Point Cloud Processing. *Proc. Computer Vision and Pattern Recognition (CVPR), IEEE* (2018).

Matthias Teschner, Bruno Heidelberger, Matthias Müller, Danat Pomerantes, and Markus H Gross. 2003. Optimized Spatial Hashing for Collision Detection of Deformable Objects. In *VMV*, Vol. 3. 47–54.

Peng-Shuai Wang, Yang Liu, Yu-Xiao Guo, Chun-Yu Sun, and Xin Tong. 2017. O-CNN: Octree-based Convolutional Neural Networks for 3D Shape Analysis. *ACM Trans. Graph.* 36, 4, Article 72 (July 2017), 11 pages.

Yue Wang, Yongbin Sun, Ziwei Liu, Sanjay E. Sarma, Michael M. Bronstein, and Justin M. Solomon. 2018. Dynamic Graph CNN for Learning on Point Clouds. (2018). arXiv:arXiv:1801.07829

Li-Yi Wei. 2008. Parallel Poisson Disk Sampling. *ACM Trans. Graph.* 27, 3, Article 20 (Aug. 2008), 9 pages.

Zhirong Wu, S. Song, A. Khosla, Fisher Yu, Linguang Zhang, Xiaoou Tang, and J. Xiao. 2015. 3D ShapeNets: A deep representation for volumetric shapes. In *2015 IEEE Conference on Computer Vision and Pattern Recognition (CVPR)*. 1912–1920.

Yifan Xu, Tianqi Fan, Mingye Xu, Long Zeng, and Yu Qiao. 2018. SpiderCNN: Deep Learning on Point Sets with Parameterized Convolutional Filters. (2018). arXiv:arXiv:1803.11527

Li Yi, Vladimir G. Kim, Duygu Ceylan, I-Chao Shen, Mengyan Yan, Hao Su, Cewu Lu, Qixing Huang, Alla Sheffer, and Leonidas Guibas. 2016. A Scalable Active Framework for Region Annotation in 3D Shape Collections. *SIGGRAPH Asia* (2016).

Li Yi, Lin Shao, Manolis Savva, Haibin Huang, Yang Zhou, Qirui Wang, Benjamin Graham, Martin Engelcke, Roman Klokov, Victor S. Lempitsky, Yuan Gan, Pengyu Wang, Kun Liu, Fenggen Yu, Panpan Shui, Bingyang Hu, Yan Zhang, Yangyan Li, Rui Bu, Mingchao Sun, Wei Wu, Minki Jeong, Jaehoon Choi, Changick Kim, Angom Geetchandra, Narasimha Murthy, Bhargava Ramu, Bharadwaj Manda, M. Ramanathan, Gautam Kumar, P. Preetham, Siddharth Srivastava, Swati Bhugra, Brejesh Lall, Christian Häne, Shubham Tulsiani, Jitendra Malik, Jared Lafer, Ramsey Jones, Siyuan Li, Jie Lu, Shi Jin, Jingyi Yu, Qixing Huang, Evangelos Kalogerakis, Silvio Savarese, Pat Hanrahan, Thomas A. Funkhouser, Hao Su, and Leonidas J. Guibas. 2017. Large-Scale 3D Shape Reconstruction and Segmentation from ShapeNet Core55. *CoRR abs/1710.06104* (2017). arXiv:1710.06104

Lequan Yu, Xianzhi Li, Chi-Wing Fu, Daniel Cohen-Or, and Pheng-Ann Heng. 2018. PU-Net: Point Cloud Upsampling Network. (2018). arXiv:arXiv:1801.06761